Biosensors and Bioelectronics 142 (2019) 111578

Contents lists available at ScienceDirect

Biosensors and Bioelectronics

journal homepage: www.elsevier.com/locate/bios

DNA nanotetrahedron-assisted electrochemical aptasensor for cardiac troponin I detection based on the co-catalysis of hybrid nanozyme, natural enzyme and artificial DNAzyme

Duanping Sun[a,b,c,d,*], Xiangan Lin[e], Jing Lu[d,**], Ping Wei[a,b,c], Zibin Luo[d], Xiange Lu[a,b,c], Zuanguang Chen[d], Luyong Zhang[a,b,c,***]

[a] Center for Drug Research and Development, Guangdong Pharmaceutical University, Guangzhou, 510006, China
[b] Guangzhou Key Laboratory of Construction and Application of New Drug Screening Model Systems, Guangdong Pharmaceutical University, Guangzhou, 510006, China
[c] Key Laboratory of New Drug Discovery and Evaluation of Ordinary Universities of Guangdong Province, Guangdong Pharmaceutical University, Guangzhou, 510006, China
[d] School of Pharmaceutical Sciences, Sun Yat-Sen University, Guangzhou, 510006, China
[e] Sun Yat-Sen Memorial Hospital, Sun Yat-Sen University, Guangzhou, 510120, China

ARTICLE INFO

Keywords:
Electrochemical biosensor
Dual aptamer
DNA nanotetrahedron
Cardiac troponin I

ABSTRACT

The sensitive and accurate detection of cardiac troponin I (cTnI) is critical for myocardial infarction diagnosis. In this work, a dual-aptamer-based electrochemical (EC) biosensor was designed for cTnI detection based on the DNA nanotetrahedron (NTH) capture probes and multifunctional hybrid nanoprobes. First, the NTH-based Tro4 aptamer probes were anchored on a screen printed gold electrode (SPGE) surface through the Au–S bond, providing an enhanced spatial dimension and accessibility for capturing cTnI. Then, the hybrid nanoprobes were fabricated by using magnetic Fe_3O_4 nanoparticles as nanocarriers to load a large amount of cTnI-specific Tro6 aptamer, natural horseradish peroxidase (HRP), HRP-mimicking Au@Pt nanozymes and G-quadruplex/hemin DNAzyme. This signaling nanoprobes are capable of specifically recognizing the target cTnI based on the Tro6 aptamer and amplifying the signals to improve the detection sensitivity via enzymatic processes. We found the remarkable enhanced effect of EC signal to be attributed to the co-catalysis effect of hybrid nanozymes, HRP and DNAzyme. The target cTnI was sandwiched between the two types of aptamers (Tro4 and Tro6) on the electrode interface. Finally, this EC aptasensing platform exhibited great analytical performance with a wide dynamic range of 0.01–100 ng mL^{-1} and a low detection limit of 7.5 pg mL^{-1} for cTnI. The high selectivity, sensitivity and reliability of EC aptasensor can provide great potential in the clinic disease diagnostics.

1. Introduction

Cardiovascular diseases are major emergent health problems worldwide. Acute myocardial infarction (AMI) can lead to irreversible heart damage and ultimately cause heart failure. Early diagnosis of possible AMI is essentially important to attenuate and prevent its progression (Nsabimana et al., 2019; Szunerits et al., 2019). In the case of heart muscle damage, cardiac protein biomarkers are released into the blood stream, including cardiac troponin (cTnC, cTnT and cTnI), myoglobin (MYO) and creatine kinase. Among those biomarkers, cTnI can reveal the tiny myocardial damage and remain in myocardial tissue for 10 days (Bakirhan et al., 2018; Steckl and Ray, 2018; Yanez-Sedeno et al., 2019). Generally, the serum level of cTnI in normal healthy persons is usually below 0.2 ng mL^{-1}. The concentration of cTnI is higher than 2.0 ng mL^{-1}, implying a direct damage of the myocardium (Szunerits et al., 2019). Therefore, cTnI has been acknowledged an ideal biomarker of myocardial cell damage for AMI diagnosis with high precision and accuracy (Chekin et al., 2018).

Recently, various methods have been reported for detecting cTnI, such as enzyme-linked immunosorbent assay (ELISA) (Bodor et al., 1992), fluorescence (Lou et al., 2018), electrochemical (EC) (Lv et al., 2019; Zhang et al., 2018), electrochemiluminescence (Wang et al., 2019; Yang et al., 2018b; Ye et al., 2019) and photoelectrochemical (Chi et al., 2019; Fan et al., 2018; Gao et al., 2019) immunoassay.

* Corresponding author. Center for Drug Research and Development, Guangdong Pharmaceutical University, Guangzhou, 510006, China.
** Corresponding author.
*** Corresponding author. Center for Drug Research and Development, Guangdong Pharmaceutical University, Guangzhou 510006, China.
E-mail addresses: sundp@gdpu.edu.cn (D. Sun), lujing0504@126.com (J. Lu), lyzhang@gdpu.edu.cn (L. Zhang).

https://doi.org/10.1016/j.bios.2019.111578
Received 25 May 2019; Received in revised form 3 August 2019; Accepted 7 August 2019
Available online 08 August 2019
0956-5663/

Compared with other methods, EC immunoassays take the advantages of miniaturization ability, short reading time, and requiring a small amount of sample. Despite the well acceptance of the immunoassay in clinical settings for cardiac biomarkers, these antibody-based immunosensors suffer from several limitations such as low stability at high temperatures and high cost for the production. Recently, aptamer-based EC biosensor has attracted special focus in the AMI analysis field (Lopa et al., 2019; Negahdary et al., 2017; Qiao et al., 2018; Sun et al., 2019). Compared to protein antibodies, aptamers are single-stranded oligonucleotides and represent a novel approach to detect biomarkers due to the superior characteristics of high stability, low cost and small size. Aptamers are also recognized as "chemical antibodies" that recognize their targets with high affinity and selectivity. For example, two kinds of aptamers (Tro4 and Tro6) have been selected as the excellent choice for the cTnI capture (Table S1) (Jo et al., 2015).

Because of the flexibility of single-stranded DNA, aptamer probes are easy to nonspecifically aggregate and entangle on the surface, which largely impede accessibility of the target (Pei et al., 2014). In order to solve the problems, DNA nanotetrahedron (NTH) has been introduced as an important biomolecular scaffold in the EC biosensor (Sun et al., 2018, 2019). DNA NTH is an artificial self-assembled nanostructure by exploiting the precise base-pairing ability of nucleic acids. Compared with single-stranded DNA probe, DNA NTH probe shows excellent specific orientation, structural stability and mechanical rigidity due to the pyramid-like organizational formation with four triangle faces and six edges (Wang et al., 2012; Yang et al., 2018a). Herein, DNA NTH can be coupled with aptamer capture probes for enhancing cTnI recognition to design the novel aptasensor.

Compared with the sandwich-type method with probe labeling, the use of NTH structure only requires a label-free method and the detection sensitivity may not meet the requirement of clinical sample analysis for cTnI. For the sandwich-type EC biosensor, a commonly used method for signal amplification is to design signaling nanoprobes by immobilizing enzymes (e.g., natural peroxidase and glucose oxidase) onto nanomaterials for improving the detection sensitivity via enzymatic processes (Lahcen and Amine, 2019; Sun et al., 2016; Zheng et al., 2014). G-quadruplex/hemin DNAzymes (GHD), a complex between a single-stranded guanine-rich nucleic acid and hemin, have been actively exploited as horseradish peroxidase (HRP)-like catalysts for EC aptasensing (Sun et al., 2015; Xu et al., 2015). Compared with natural enzymes, artificial DNAzymes have the striking merits of simple synthesis, cost-effectiveness, and easy modification (Tang et al., 2012). By using combination of natural HRP and DNAzymes is a good choice for improving detection sensitivity.

Nanomaterials are not only useful to load enzymes with high surface, but also possess enzyme-mimicking properties for signal amplification (Farzin et al., 2018). Recently, nanozymes, nanomaterial with enzyme-like properties, have known as a new kind of enzymes due to its outstanding advantages of robustness, mass production and low cost (Wei and Wang, 2013; Wu et al., 2019). To date, a large amount of nanomaterials have been demonstrated to possess the HRP-like properties, ranging from metals and metal oxides to metal organic frameworks. For instance, magnetic iron oxide (Fe_3O_4) nanoparticles (NPs) and core-shell bimetallic NPs possess an intrinsic enzyme-mimicking activity similar to that of natural HRP (Yuan et al., 2017; Zhang et al., 2015). Therefore, by the combination of Fe_3O_4 nanozymes (Zheng et al., 2014) and Au@Pt NPs nanozymes (Wu et al., 2016), the hybrid nanoelectrocatalysts (nanozymes) can be used as a promising nanocarrier to load HRP and DNAzyme for sensitive aptasensing.

In this work, we designed an EC dual-aptamer biosensor for cTnI analysis by using the DNA NTH-based Tro4 aptamer probes and multifunctional nanoprobes for signal amplification. First, the thiolated NTH-Tro4 capture probes were attached to the screen-printed gold electrode (SPGE) surface via thiol − gold interactions. It can provide a solution-native-like recognition interface for the greatly enhanced recognition of cTnI. Then, the multifunctional nanoprobes were fabricated by using the Tro6 aptamer, HRP and HRP-mimicking GHD immobilized on the surfaces of hybrid Fe_3O_4/Au@Pt nanozymes. The cTnI can be recognized to fabricate an NTH-Tro4/cTnI/nanoprobes sandwich structure on a SPGE surface. The integration of hybrid nanozymes, HRP and DNAzyme has greatly improved the detection sensitivity of the EC aptasensing system. The combined utilization of NTH-Tro4 aptamer probes and Fe_3O_4/Au@Pt-HRP-DNAzyme-Tro6 hybrid nanoprobes can significantly enhance the specific recognition and the detection sensitivity for cTnI. Finally, the EC dual-aptamer-based biosensor was successfully explored for ultrasensitive and selective determination of the AMI marker cTnI.

2. Experimental section

2.1. Reagents and apparatus

Recombinant human cardiac troponin I (cTnI, NO. RPA478Hu01), recombinant human myoglobin (MYO, NO. RPA480Hu01), recombinant human hyaluronan synthase 1 (HAS1, NO. RPC520Hu01), bovine serum albumin (BSA) and ELISA kit for cTnI (NO. SEA478Hu) were all purchased from Cloud-clone Co., Ltd. (Wuhan, China). Recombinant human epidermal growth factor receptor 2 (HER2, NO. ab182691) was obtained from Abcam Co., Ltd (Cambridge, USA). All oligonucleotides were synthesized and purified by Invitrogen Biotech. Co., Ltd. (Shanghai, China). The sequences were showed in Table S2.

EC impedance spectroscopy (EIS), cyclic voltammetry (CV), and differential pulse voltammetry (DPV) were carried out by using a RST5100F workstation (Suzhou Risetest Instrument Co., Ltd., Suzhou, China). The EC detection was performed on disposable SPGE with 4 mm diameter working area (DropSens, LIanera, Spain) or glassy carbon electrode (GCE) with 3 mm diameter working area (Gaossunion Technology Co., Ltd., Wuhan, China). Other detailed chemicals and apparatus are provided in the Supplementary material.

2.2. Fabrication of hybrid nanoprobes

According to the reported methods, poly(diallyldimethylammonium chloride) modified Fe_3O_4 (Fe_3O_4/PDDA), Au@Pt NPs and Fe_3O_4/PDDA/Au@Pt nanomaterials were prepared. Detailed steps are provided in the Supplemental material. The pH value of the colloidal suspension of Fe_3O_4/PDDA/Au@Pt NPs was adjusted to 9.0. In the pH 9.0 solution, the fabricated Fe_3O_4/PDDA/Au@Pt NPs had a good dispersion. Then 50 μL of HRP (1 mg mL^{-1}) and 50 μL of thiolated DNA probe (5 μM) was added to the dispersion, and the mixture was stirred mechanically overnight at 4 °C. HRP can be immobilized onto the Fe_3O_4/PDDA/Au@Pt NPs via metal − thiol interactions due to the presence of cysteine residues in HRP. In the presence of K^+, the G-rich DNA folded into the G-quadruplex structure, and then hemin can bind to the G-quadruplex structure for forming HRP–mimicking GHD. Subsequently, hemin (0.1 mg) was added into the phosphate buffered saline (PBS, 100 mM, pH 7.0, K^+) at 4 °C for 2 h to form GHD. The reaction mixture was washed with PBS solution for several times. Finally, the obtained Fe_3O_4/PDDA/Au@Pt–HRP–GHD–Tro6 nanoprobes were redispersed in 10 mM PBS solution and stored at 4 °C for further use.

2.3. Fabrication of the EC aptasensor

Before the assembly of NTH, the monomers (A, B, C and D) were pretreated with 10 mM tris(2-carboxyethyl) phosphine hydrochloride (TCEP) for 2 h to cleave the disulfide linkage. The DNAs were mixed equivalently in TM buffer (10 mM Tris-HCl, 50 mM Mg^{2+}, pH 8.0), heated at 95 °C for 10 min, and rapidly cooled at 4 °C for 10 min. The formation of DNA nanostructures can be analyzed using 3% agarose gel electrophoresis.

The SPGEs were ultrasonic cleaned in ethanol and ultrapure water

for 2 times, respectively. Then the bare SPGE surface was electrochemically cleaned in 0.5 M H_2SO_4 scanning between −0.2 and 1.5 V until a stable CV was obtained. 10 μL of 1.25 μM NTH-Tro4 capture probe was dropped on the SPGE surface for 4 h. The DNA modified SPGE was washed with ultrapure water to remove the unbound aptamer probe. Then 10 μL of 1 mM 6-mercapto-1-hexanol (MCH) was dropped onto the SPGE surface to block the blank sites for 1 h at room temperature. Unbound MCH was thoroughly washed away with PBS solution.

The modified electrode was incubated with 100 μL of cTnI with different concentrations at 37 °C for 60 min for capturing cTnI specifically. The cTnI-captured electrode was washed with PBS solution carefully to remove the non-captured cTnI. Afterward, 10 μL of hybrid nanoprobes were dropped and incubated at 37 °C for 60 min to form sandwich-type aptasensor and washed thoroughly with 10 mM PBS to remove nonspecifically bound conjugates. The prepared electrode was immersed in degassed PBS (pH 7.0, 100 mM) containing 3 mM hydroquinone (HQ) and 2 mM H_2O_2 and reacted for 5 min. The DPV measurements was performed with potential ranging from +0.1 to −0.3 V, a pulse amplitude of 50 mV and a pulse time of 50 ms.

3. Results and discussion

3.1. Principle of the EC aptasensor

In this work, the hybrid electrocatalysts were fabricated via a layer-by-layer assembly process. Fe_3O_4 NPs possess an intrinsic enzyme-like catalytic activity similar to that of natural HRP. PDDA was performed for fabricating the shell over the Fe_3O_4 NPs to form Fe_3O_4/PDDA beads. In addition, Au@Pt bimetallic NPs were also synthesized and both Fe_3O_4 NPs and Au@Pt NPs exhibit the HRP-mimicking activities toward H_2O_2 reduction with large surface area. The Au@Pt NPs were attached to the surface of the Fe_3O_4/PDDA NPs for forming Fe_3O_4/PDDA/Au@Pt nanozymes based on the electrostatic interactions. The hybrid nanomaterials (nanozymes) were utilized as nanocarriers to load thiolated DNA probe and HRP for fabricating signal nanoprobes. Furthermore, the thiolated capture probes consist of the sequences of Tro6 aptamer and G-quadruplex. With the aid of hemin and K^+, the HRP-mimicking GHD can be formed. As a result, the designed nanoprobes are capable of amplifying the EC signal with the integration of hybrid nanozymes, natural HRP and artificial DNAzyme, and capturing the target cTnI with the Tro6 aptamer.

As shown in Scheme 1, the NTH-based Tro4 aptamer probe was attached on the SPGE surface to efficiently recognize the target cTnI with optimized interface density and steady support. After the target cTnI was captured, the hybrid nanoprobes (Fe_3O_4/PDDA/Au@Pt–HRP–DNAzyme–Tro6) were assembled to fabricate a NTH-Tro4/cTnI/nanoprobes sandwich-like structure. After the modified electrode was immersed in the detection solution, the HQ can be oxidized to benzoquinone (BQ) with H_2O_2 in the enzymatic reaction, which was catalyzed by numerous HRP, HRP-like nanozymes and DNAzymes. Finally, the BQ can be reduced back to HQ by receiving electrons from the electrode. Such co-catalysis can greatly improve the sensitivity of the proposed EC aptasensor. The process is shown as below

$$H_2O_2 + H_2Q \rightarrow Q + 2H_2O$$

$$Q + 2H^+ + 2e^- \rightarrow H_2Q$$

where H_2Q is HQ and Q is BQ (Chen et al., 2014; Liu et al., 2012). The EC signal was related to the amount of hybrid nanoprobes on the electrode interface, further related to the concentration of cTnI.

3.2. Characterization of the nanomaterials

Ultraviolet visible (UV–Vis), transmission electron microscopy (TEM), scanning electron microscopy (SEM) and fourier transform infra-red (FT-IR) analysis were utilized to characterize Au@Pt NPs and Fe_3O_4 NPs. As shown in Fig. S1A, the AuNPs exhibited a strong localized surface plasmon resonance (LSPR) peak at 520 nm. However, the LSPR peak of Au@Pt NPs is blue-shifted to 508 nm. According to the previous studies, the blue-shift is attributed to the existence of Pt shells on the AuNPs. As we can see from Fig. 1A and B, the synthesized Au@Pt NPs had good dispersion and uniform particle size with 13.5 nm. These results indicated the successful synthesis of Au@Pt NPs.

As can be seen from the FT-IR spectra of Fe_3O_4 NPs in Fig. S1B, the absorption peak at 575 cm^{-1} is assigned to the Fe–O stretching vibrations in iron oxide. The observed bands at 1621 and 1410 cm^{-1} correspond to the symmetric C–O stretching and the asymmetric stretching of COO^-, respectively. The absorption peak appearing at 3407 cm^{-1} is associated with vibrations of OH of the absorbed water molecules. The results of Fig. 1C and D confirm that the synthesized Fe_3O_4 NPs were spherical and the diameter of Fe_3O_4 NPs is a narrow particle size distribution with 105 nm. These results demonstrated that the Fe_3O_4 NPs were synthesized successfully.

The surfaces of the Fe_3O_4 NPs were negatively charged at neutral pH with carboxyl groups. The adsorption of positively charged PDDA on colloidal Fe_3O_4 NPs switched the ζ potential to a positive value. Au@Pt NPs with negatively charged interfaces can be attached electrostatically to the surface of the Fe_3O_4/PDDA NPs (Fig. S2). As shown by the SEM image in Fig. 1E, a monolayer of Au@Pt NPs was covered on the Fe_3O_4/PDDA bead to form a core-satellite nanostructure. At the same time, the energy dispersive spectroscopy (EDS) line scanning data and elemental mapping analysis revealed that the elements of Fe, O, Au and Pt were indispensable for the hybrid nanomaterials (Figs. S3 and S4). As exhibited in Fig. 1F, the Fe_3O_4/PDDA/Au@Pt nanocomposites exhibited a slightly larger size than that of the Fe_3O_4 NPs. Hence, the results indicated that the Fe_3O_4/PDDA/Au@Pt electrocatalysts had been successfully synthesized.

In addition, the HRP-mimicking catalytic properties of Fe_3O_4/PDDA/Au@Pt NPs were also verified. Fig. S5 compared the typical CVs of the bare GCE and nanocomposites modified GCE for H_2O_2 reduction in N_2-saturated 100 mM PBS containing 10 mM H_2O_2. As judged from the onset potential and measured current for H_2O_2 reduction, the peak current of GCE/Fe_3O_4/PDDA/Au@Pt (curve c) showed much higher than that of the GCE (curve a) and GCE/Fe_3O_4 (curve b). It proved that Fe_3O_4/PDDA/Au@Pt NPs can efficiently catalyze the EC reduction of H_2O_2 with HRP-like activity.

3.3. Characterization of the NTH-based aptamer probe

Tro4 and Tro6 aptamer (Table S1 and Fig. S6) were selected to capture the target cTnI. As shown in Fig. S7A, DNA NTH structure, assembled from four single-stranded DNA with ordered probe arrangement and distribution, can be utilized to increase the target accessibility and further improve detection performance. With thiol groups at three vertices and the fourth vertex containing exposed Tro4 aptamer probe, the thiol-modified NTH can be firmly anchored on the SPGE interface uniformly by the strong interaction between Au and thiol. Briefly, Tro4 aptamers are built into one of the NTH sequences (D), and the other three DNA with thiol groups (A, B and C) can be anchored on the gold electrode.

DNA NTH structure was demonstrated by the agarose gel electrophoretic (Fig. S7B). The NTH-Tro4 (lane 4) migrated more slowly than combinations constructed of fewer than four single-stranded sequences (lane 1, lane 2 and lane 3). As the rapid and specific DNA hybridization ensuring the high yield of NTHs, the only major clear band can be observed on the gel. Therefore, the results indicated the NTH-Tro4 aptamer probes ha been successfully fabricated.

3.4. EC characterization of the EC aptasensor

EIS is a label-free and direct detection method to quantify the target

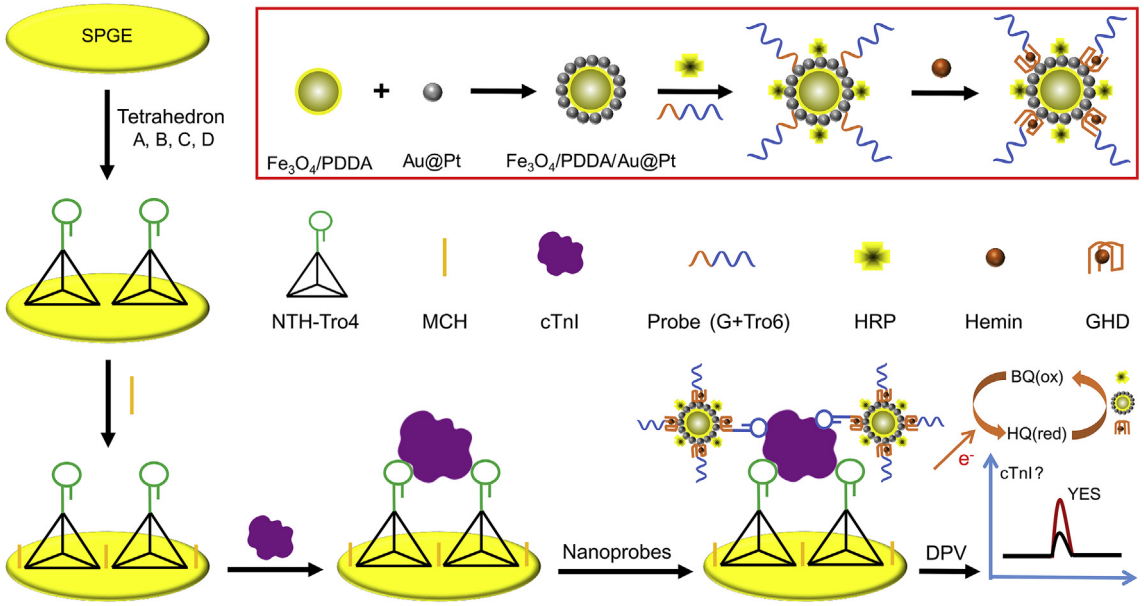

Scheme 1. Schematic illustration of the assembly process of the Fe_3O_4/PDDA/Au@Pt-HRP-DNAzyme-Tro6 signaling nanoprobes and the construction process of the EC aptasensor for cTnI detection.

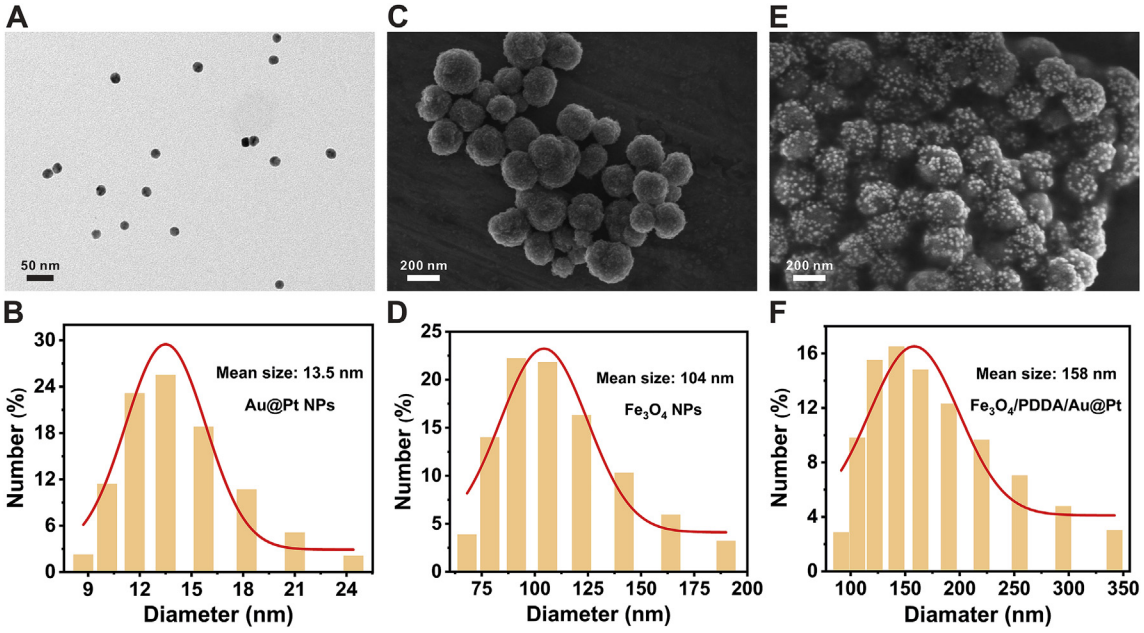

Fig. 1. TEM image of the Au@Pt NPs (A). SEM images of Fe_3O_4 NPs (C) and Fe_3O_4/PDDA/Au@Pt NPs (E). Size distribution of Au@Pt NPs with average diameters of 13.5 nm (B), Fe_3O_4 NPs with average diameters of 104 nm (D) and Fe_3O_4/PDDA/Au@Pt NPs with average diameters of 158 nm (F).

molecules and to measure interfacial molecular interactions. EIS was performed to understand the characterization of this aptasensor (Fig. 2). In the Nyquist plot, the semicircle diameter of the EIS is proportional to the charge-transfer resistance of the electrode interface. For the bare SPGE, the Nyquist plot included no semicircle domain (curve a). When the SPGE was modified by the NTH-based Tro4 aptamer, a small semicircle was observed (curve b), suggesting the electron transfer was blocked by the nonconductive DNA. With further the modification of MCH, the electron-transfer resistance on the SPGE surface increased (curve c). When the target cTnI was captured by the aptamer probe modified SPGE, a larger increase of the semicircle diameter can be seen due to the difficulty of charge transfer (curve d). These results indicated that the NTH-Tro4 aptamer can specifically recognize cTnI and successful assembled process occurred on the SPGE surface step by step.

DPV was utilized to demonstrate the signal amplification strategy of the EC aptasensor. As depicted in Fig. 3A, when the SPGE/NTH-Tro4/MCH/cTnI/Fe_3O_4/PDDA/Au@Pt-Tro6 was immersed in the PBS buffer with 2 mM H_2O_2 and 3 mM HQ, a weak DPV reduction peak appeared, which was ascribed to the BQ generated by the catalysis of Fe_3O_4/PDDA/Au@Pt hybrid nanozymes. Compared with the peak current of the Fe_3O_4/PDDA/Au@Pt-Tro6 signaling nanoprobes (curve a), the Fe_3O_4/PDDA/Au@Pt-HRP-Tro6 nanoprobes with the natural HRP and hybrid nanozymes catalyzed oxidation of the HQ with H_2O_2 and amplified the EC signals obviously (curve b). As can be seen from Fig. 3B, when the SPGE/NTH-Tro4/MCH without target cTnI was immersed in the PBS buffer with 2 mM H_2O_2 and 3 mM HQ, a very tiny EC responses can be observed for cTnI detection (curve d). However, the peak current

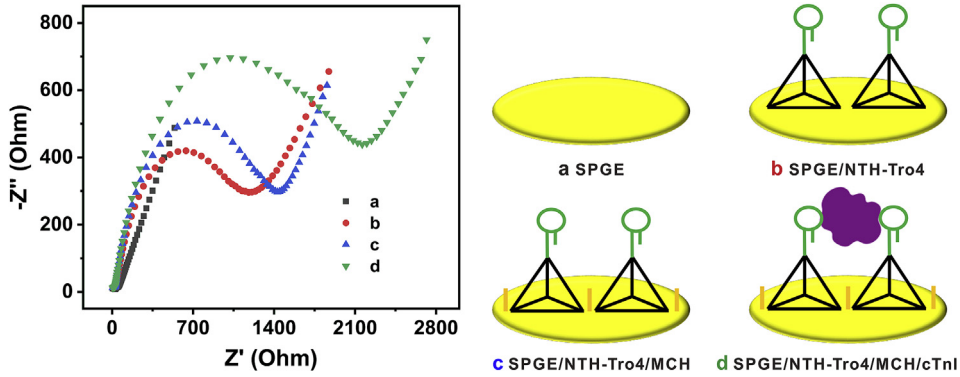

Fig. 2. EIS of (a) bare SPGE, (b) SPGE/NTH-Tro4, (c) SPGE/NTH-Tro4/MCH, and (d) SPGE/NTH-Tro4/MCH/cTnI in 0.5 M KCl solution containing 5 mM $[Fe(CN)_6]^{4-/3-}$ (impedance spectral frequency 0.1–10^5 Hz, amplitude 10 mV, cTnI concentration 10 ng mL^{-1}).

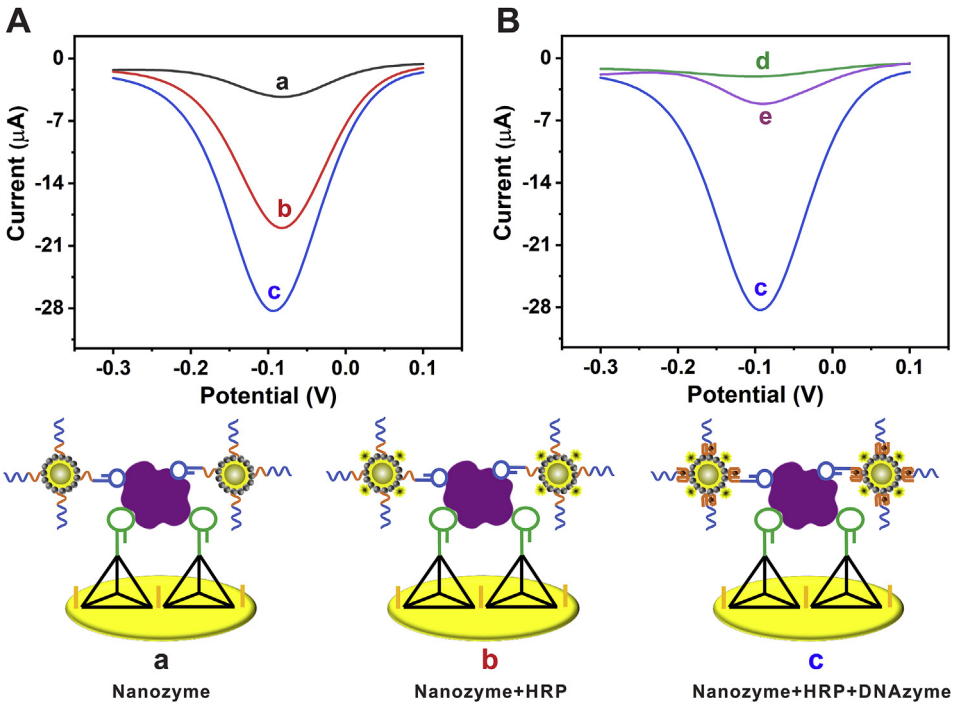

Fig. 3. (A) DPV responses of the SPGE/NTH-Tro4/MCH/cTnI with Fe_3O_4/PDDA/Au@Pt-Tro6 nanoprobes (a), Fe_3O_4/PDDA/Au@Pt-HRP-Tro6 nanoprobes (b), and Fe_3O_4/PDDA/Au@Pt-HRP- GHD-Tro6 nanoprobes (c). (B) DPV responses of the SPGE/NTH-Tro4/MCH (the background DPV, the modified electrode without target cTnI, curve d), blank signal (the modified electrode after incubation in Fe_3O_4/PDDA/Au@Pt-HRP-GHD-Tro6 nanoprobes without target cTnI, curve e), and the SPGE/NTH-Tro4/MCH/cTnI/Fe_3O_4/PDDA/Au@Pt-HRP-GHD-Tro6 (c). The DPV measurements were performed in the 100 mM PBS (pH 7.0) solution with 3 mM HQ and 2 mM H_2O_2 (amplitude 50 mV, incubation time 60 min, cTnI concentration 10 ng mL^{-1}).

increased sharply after incubation of the SPGE/NTH-Tro4/MCH in Fe_3O_4/PDDA/Au@Pt-HRP-GHD-Tro6 nanoprobes without target cTnI (curve e). A small amount of nanoprobes can be absorbed on the modified SPGE electrode. For the SPGE/NTH-Tro4/MCH/cTnI/Fe_3O_4/PDDA/Au@Pt-HRP-GHD-Tro6, the largest peak current can be observed due to the co-catalysis of hybrid nanozyme, natural HRP and DNAzyme (curve c). These results demonstrated that the hybrid nanoprobes can largely enhance the DPV signal and improve the detection sensitivity by efficiently capturing cTnI and catalyzing the HQ with H_2O_2.

The effects of the incubation time of cTnI and nanoprobes on the EC responses were investigated to optimize the analytical performance of the aptasensor. The cTnI solution (10 ng mL^{-1}) was dropped onto the SPGE and incubated for different times (30, 40, 50, 60, and 70 min). In Fig. S8, the DPV current signal increased along increasing the incubation time. However, the maximum signal was achieved at 60 min. Hence, 60 min was used as the optimal incubation time for cTnI and nanoprobes in subsequent experiments.

3.5. Performance of the EC aptasensor

Different concentrations of the cTnI were detected under the optimum conditions. Fig. S9A showed that the DPV peak currents increased with the increase of cTnI concentrations based on the Fe_3O_4/PDDA/Au@Pt-HRP-Tro6 signaling nanoprobes. DPV response (I) was linearly related to the logarithm of cTnI concentration (C_{cTnI}) with a linear range of 0.01–100 ng mL^{-1}. As depicted in Fig. S9B, the linear regression equation is I (μA) = 14.88 + 4.59 lgC_{cTnI} (ng mL^{-1}) with a correlation coefficient of 0.997 (standard deviations of slope and y-intercept were 0.18 and 0.30). The limit of detection (defined as LOD = 3σ/m, where σ is the standard deviation of the blank and m is the slope of the corresponding calibration curve) is calculated to be 8.8 pg mL^{-1} for cTnI.

Moreover, Fig. 4A showed the DPV peak current responses with the increase of cTnI concentrations from 0.01 to 100 ng mL^{-1} based on the co-catalysis of hybrid nanozyme, natural HRP and artificial DNAzyme. As shown in Fig. 4B, the linear regression equation is I (μA) = 22.14 + 7.82 lgC_{cTnI} (ng mL^{-1}) with a correlation coefficient of 0.996 (standard deviations of slope and y-intercept were 0.35 and 0.57). The estimated LOD is 7.5 pg mL^{-1} for cTnI based on the 3σ method. It is obvious that the LOD of EC aptasensor exhibited lower than that of the previous method based on the co-catalysis of hybrid nanozyme and natural HRP. In addition, compared with the most of the previously reported aptamer-based methods and ELISA kit (Table S3),

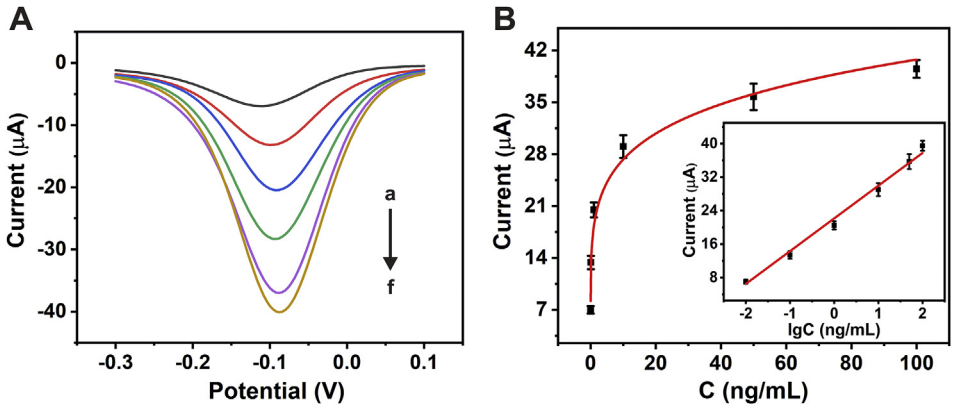

Fig. 4. (A) DPV responses to different concentrations of target cTnI (a–f: 0.01 ng mL^{-1}, 0.1 ng mL^{-1}, 1 ng mL^{-1}, 10 ng mL^{-1}, 50 ng mL^{-1} and 100 ng mL^{-1}) based on the Fe_3O_4/PDDA/Au@Pt-HRP-GHD-Tro6 signaling nanoprobes. (B) Variation of the peak current as a function of cTnI concentration (the allometric model: I (μA) = 18.26 $C_{cTnI}^{0.17}$). Inset: the linear relationship of currents versus the logarithm of cTnI concentration in the range from 0.01 ng mL^{-1} to 100 ng mL^{-1}.

the proposed EC aptasensor exhibited a wider detection range and lower LOD for cTnI.

Then, the reproducibility of the EC aptasensor was evaluated with the data from five independent EC measurements. When the concentration of cTnI was 10 ng/mL, the EC aptasensor performed a relative standard deviation (RSD) value of 5.3%. The result demonstrated that the repeatability and precision of the established EC methods were acceptable.

To prove the selectivity of the aptasensor, some interfering proteins, such as BSA, HAS1, HER2 and MYO, were introduced. The concentration of cTnI was chosen as 0.1 ng mL^{-1} and the concentration of the interfering proteins were chosen as 10 ng mL^{-1}. As shown in Fig. 5A and B, the introduction of BSA, HAS1, HER2, MYO had a negligible effect on the EC signal, while the DPV responses were increased obviously for cTnI and the mixture of cTnI and nonspecific proteins. The cTnI had a similar DPV response with the mixture of cTnI and nonspecific proteins. These results illustrated the EC aptasensor possessed excellent selectivity toward cTnI detection.

3.6. Determination of cTnI in human serum sample

Recovery experiments were performed for investigating the practicability of the proposed EC aptasensor. Different concentrations of cTnI were spiked in 5% real human serum with 10 mM PBS solution. The prepared sample solution was incubated with the proposed aptasensor to test the EC signal. As shown in Table S4, the EC aptasensor showed great performance with the recovery values of 97–105.3% and the RSD values of 4.5%–5.2%.

The practical application of the EC aptasensor was further investigated by detecting cTnI in the human serum samples of patients. As shown in Table S5, the concentrations of cTnI in the diluted serum sample obtained with this aptasensor were consistent with those determined by ELISA kit. All these results indicated that the proposed EC aptasensor can detect cTnI in human serum samples with high accuracy.

4. Conclusions

In conclusion, an ultrasensitive EC dual-aptamer-based biosensor was designed for the determination of cTnI on the basis of three-dimensional DNA NTH structure and multifunctional hybrid nanoprobes. NTH-Tro4 capture probes can improve the enhanced capture of cTnI with optimized interface density and steady support. Furthermore, with the help of hybrid nanozymes, HRP and HRP-mimicking DNAzyme, the fabricated aptasensor showed a wide linear concentration range (10 pg mL^{-1} to 100 ng mL^{-1}) and a low LOD (7.5 pg mL^{-1}) for cTnI. The EC aptasensor has great potential in the clinic disease diagnostics for AMI with good sensitivity, selectivity and reproducibility. However, one of the challenges for the EC aptasensing of cTnI concerns sensitive recording in complex media other than human serum such as sweat or saliva where lower detection limits are required.

Declaration of competing interest

The authors declare that they have no known competing financial interests or personal relationships that could have appeared to influence the work reported in this paper.

Conflict of interest

The author(s) declare that they have no conflict of interest.

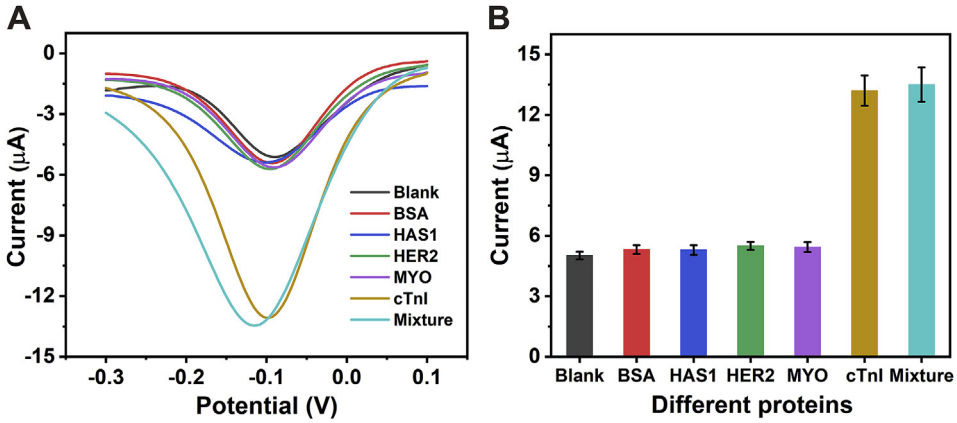

Fig. 5. DPV responses (A) and the corresponding histogram (B) to different proteins, including BSA (10 ng mL^{-1}), HAS1 (10 ng mL^{-1}), HER2 (10 ng mL^{-1}), MYO (10 ng mL^{-1}), cTnI (0.1 ng mL^{-1}), and the mixture (containing all the proteins) (incubation time 60 min).

CRediT authorship contribution statement

Duanping Sun: Conceptualization, Funding acquisition, Investigation, Methodology, Supervision, Validation, Writing - original draft, Writing - review & editing. **Xiangan Lin:** Data curation, Resources. **Jing Lu:** Formal analysis, Funding acquisition, Resources, Software, Writing - original draft, Writing - review & editing. **Ping Wei:** Formal analysis. **Zibin Luo:** Visualization. **Xiange Lu:** Data curation. **Zuanguang Chen:** Funding acquisition. **Luyong Zhang:** Funding acquisition, Project administration.

Acknowledgments

This work was supported by the National Natural Science Foundation of China (No. 81803521 and 21675177), the Natural Science Foundation of Guangdong Province (No. 2018A030310142), the Fundamental Research Funds for the Central Universities (No. 18zxxt69), the Guangzhou Key Laboratory of Construction and Application of New Drug Screening Model Systems (No. 201805010006), the Key Laboratory of New Drug Discovery and Evaluation of Ordinary Universities of Guangdong Province (No. 2017KSYS002), and a Start-up Grant from Guangdong Pharmaceutical University (No. 51377003). The authors acknowledge the help from Dr. Xiangan Lin in Sun Yat-Sen Memorial Hospital for providing patient samples.

Appendix A. Supplementary data

Supplementary data to this article can be found online at https://doi.org/10.1016/j.bios.2019.111578.

References

Bakirhan, N.K., Ozcelikay, G., Ozkan, S.A., 2018. J. Pharmaceut. Biomed. 159, 406–424.
Bodor, G.S., Porter, S., Landt, Y., Ladenson, J.H., 1992. Clin. Chem. 38, 2203–2214.
Chekin, F., Vasilescu, A., Jijie, R., Singh, S.K., Kurungot, S., Iancu, M., Badea, G., Boukherroub, R., Szunerits, S., 2018. Sens. Actuators B Chem. 262, 180–187.
Chen, X.J., Wang, Y.Z., Zhang, Y.Y., Chen, Z.H., Liu, Y., Li, Z.L., Li, J.H., 2014. Anal. Chem. 86, 4278–4286.
Chi, H.T., Han, Q.Z., Chi, T.H., Xing, B., Ma, N., Wu, D., Wei, Q., 2019. Biosens. Bioelectron. 132, 1–7.
Fan, D.W., Bao, C.Z., Khan, M.S., Wang, C.L., Zhang, Y., Liu, Q.Z., Zhang, X., Wei, Q., 2018. Biosens. Bioelectron. 106, 14–20.
Farzin, L., Shamsipur, M., Samandari, L., Sheibani, S., 2018. J. Pharmaceut. Biomed. 161, 344–376.
Gao, C.M., Xue, J., Zhang, L.N., Zhao, P.N., Cui, K., Ge, S.G., Yu, J.H., 2019. Biosens. Bioelectron. 131, 17–23.
Jo, H., Gu, H., Jeon, W., Youn, H., Her, J., Kim, S.K., Lee, J., Shin, J.H., Ban, C., 2015. Anal. Chem. 87, 9869–9875.
Lahcen, A.A., Amine, A., 2019. Electroanalysis 31, 188–201.
Liu, Y., Liu, Y., Feng, H., Wu, Y., Joshi, L., Zeng, X., Li, J., 2012. Biosens. Bioelectron. 35, 63–68.
Lopa, N.S., Rahman, M.M., Ahmed, F., Ryu, T., Sutradhar, S.C., Lei, J., Kim, J., Kim, D.H., Lee, Y.H., Kim, W., 2019. Biosens. Bioelectron. 126, 381–388.
Lou, D.D., Fan, L., Cui, Y., Zhu, Y.F., Gu, N., Zhang, Y., 2018. Anal. Chem. 90, 6502–6508.
Lv, H., Li, Y.Y., Zhang, X.B., Li, X.J., Xu, Z., Chen, L., Li, D.G., Dong, Y.H., 2019. Biosens. Bioelectron. 133, 72–78.
Negahdary, M., Behjati-Ardakani, M., Sattarahmady, N., Yadegari, H., Heli, H., 2017. Sens. Actuators B Chem. 252, 62–71.
Nsabimana, A., Ma, X.G., Yuan, F., Du, F.X., Abdussalam, A., Lou, B.H., Xu, G.B., 2019. Electroanalysis 31, 177–187.
Pei, H., Zuo, X.L., Zhu, D., Huang, Q., Fan, C.H., 2014. Accounts Chem. Res. 47, 550–559.
Qiao, X.J., Li, K.X., Xu, J.Q., Cheng, N., Sheng, Q.L., Cao, W., Yue, T.L., Zheng, J.B., 2018. Biosens. Bioelectron. 113, 142–147.
Steckl, A.J., Ray, P., 2018. ACS Sens. 3, 2025–2044.
Sun, D.P., Lu, J., Chen, Z.G., Yu, Y.Y., Mo, M.N., 2015. Anal. Chim. Acta 885, 166–173.
Sun, D.P., Lu, J., Luo, Z.F., Zhang, L.Y., Liu, P.Q., Chen, Z.G., 2018. Biosens. Bioelectron. 120, 8–14.
Sun, D.P., Lu, J., Zhong, Y.W., Yu, Y.Y., Wang, Y., Zhang, B.B., Chen, Z.G., 2016. Biosens. Bioelectron. 75, 301–307.
Sun, D.P., Luo, Z.B., Lu, J., Zhang, S.S., Che, T., Chen, Z.G., Zhang, L.Y., 2019. Biosens. Bioelectron. 134, 49–56.
Szunerits, S., Mishyn, V., Grabowska, I., Boukherroub, R., 2019. Biosens. Bioelectron. 131, 287–298.
Tang, J., Hou, L., Tang, D.P., Zhang, B., Zhou, J., Chen, G.N., 2012. Chem. Commun. 48, 8180–8182.
Wang, S.S., Zhao, Y.Y., Wang, M.M., Li, H.J., Saqib, M., Ge, C.H., Zhang, X.D., Jin, Y.D., 2019. Anal. Chem. 91, 3048–3054.
Wang, Z.G., Xue, Q.W., Tian, W.Z., Wang, L., Jiang, W., 2012. Chem. Commun. 48, 9661–9663.
Wei, H., Wang, E.K., 2013. Chem. Soc. Rev. 42, 6060–6093.
Wu, J.J.X., Wang, X.Y., Wang, Q., Lou, Z.P., Li, S.R., Zhu, Y.Y., Qin, L., Wei, H., 2019. Chem. Soc. Rev. 48, 1004–1076.
Wu, Z., Fu, Q.Q., Yu, S.T., Sheng, L.R., Xu, M., Yao, C.Z., Xiao, W., Li, X.Q., Tang, Y., 2016. Biosens. Bioelectron. 85, 657–663.
Xu, W.J., Xue, S.Y., Yi, H.Y., Jing, P., Chai, Y.Q., Yuan, R., 2015. Chem. Commun. 51, 1472–1474.
Yanez-Sedeno, P., Campuzano, S., Pingarron, J.M., 2019. Chem. Commun. 55, 2563–2592.
Yang, F., Zuo, X.L., Fan, C.H., Zhang, X.E., 2018a. Natl. Sci. Rev. 5, 740–755.
Yang, X., Yu, Y.Q., Peng, L.Z., Lei, Y.M., Chai, Y.Q., Yuan, R., Zhuo, Y., 2018b. Anal. Chem. 90, 3995–4002.
Ye, J., Zhu, L.P., Yan, M.X., Zhu, Q.J., Lu, Q.Q., Huang, J.S., Cui, H., Yang, X.R., 2019. Anal. Chem. 91, 1524–1531.
Yuan, Y.L., Li, S.S., Xue, Y.W., Liang, J.T., Cui, L.J., Li, Q.B., Zhou, S.F., Huang, Y., Li, G.Y., Zhao, Y.X., 2017. Anal. Biochem. 534, 56–63.
Zhang, C.X., Shen, G.Y., Shen, Y.M., Zhang, X.Y., 2015. Anal. Biochem. 485, 66–71.
Zhang, T., Ma, N., Ali, A., Wei, Q., Wu, D., Ren, X., 2018. Biosens. Bioelectron. 119, 176–181.
Zheng, T.T., Zhang, Q.F., Feng, S., Zhu, J.J., Wang, Q., Wang, H., 2014. J. Am. Chem. Soc. 136, 2288–2291.